

Modelling of monovacancy diffusion in W over wide temperature range

L. Bukonte,^{a)} T. Ahlgren, and K. Heinola

Department of Physics, University of Helsinki, P.O. Box 43, 00014 Helsinki, Finland

(Received 11 November 2013; accepted 13 March 2014; published online 25 March 2014)

The diffusion of monovacancies in tungsten is studied computationally over a wide temperature range from 1300 K until the melting point of the material. Our modelling is based on Molecular Dynamics technique and Density Functional Theory. The monovacancy migration barriers are calculated using nudged elastic band method for nearest and next-nearest neighbour monovacancy jumps. The diffusion pre-exponential factor for monovacancy diffusion is found to be two to three orders of magnitude higher than commonly used in computational studies, resulting in attempt frequency of the order 10^{15} Hz. Multiple nearest neighbour jumps of monovacancy are found to play an important role in the contribution to the total diffusion coefficient, especially at temperatures above $2/3$ of T_m , resulting in an upward curvature of the Arrhenius diagram. The probabilities for different nearest neighbour jumps for monovacancy in W are calculated at different temperatures. © 2014 AIP Publishing LLC. [<http://dx.doi.org/10.1063/1.4869497>]

I. INTRODUCTION

Tungsten (W) is one of the strongest candidates to be used as the divertor plate material for next step fusion device (ITER) due to its high melting point, low erosion rate, good thermal conductivity, and low hydrogen retention. Such combination of properties makes W a promising plasma-facing wall material. However, continuous bombardment with high energy neutrons (~ 14 MeV) introduces defects in plasma facing materials. Open volume defects, such as vacancies, are known to trap hydrogen (H) and thus are the main reasons for H retention in W. In fusion reactors, this is a critical safety issue due to tritium retention. Moreover, the concentration and the mobility of vacancies affect the microstructure of materials and, therefore, also their mechanical and thermal properties.

From statistical thermodynamics, the Gibbs free energy

$$\Delta G_v^f = \Delta H_v^f - T\Delta S_v^f \quad (1)$$

expressed in terms of formation enthalpy (H_v^f) and the formation entropy (S_v^f), corresponds to the work required to create a vacancy, simultaneously creating an adatom at the surface.

At equilibrium, the site fraction of vacancies in the crystal at constant pressure is given by equation,

$$c_v(T) = \exp\left(\frac{-G_v^f}{k_B T}\right) = \exp\left(\frac{-H_v^f(T) + TS_v^f(T)}{k_B T}\right). \quad (2)$$

The vacancy formation enthalpy close to the surface can be calculated as

$$H_v^f = E_{vac} - \left(\frac{N-1}{N}\right)E_0, \quad (3)$$

where E_{vac} is the total energy of simulation cell with one vacancy, N —number of atoms in perfect simulation cell, and E_0 —the total energy of the system without defects.

^{a)}laura.bukonte@helsinki.fi

Experimentally obtained equilibrium vacancy fraction near the melting point ($T_m = 3695$ K) in W is $\sim 10^{-4}$,² giving vacancy formation energy of about 3.5 eV, which is in agreement with density functional theory calculations.³

The migration of vacancies is the dominant mechanism behind self-diffusion in most FCC and BCC metals.¹ It is strongly temperature dependent and is often expressed in Arrhenius form,

$$D = D_0 \exp\left(\frac{-H_v^m}{k_B T}\right), \quad (4)$$

where D_0 is the pre-exponential factor, H_v^m —the migration enthalpy, k_B —the Boltzmann constant, and T —the absolute temperature. The diffusion pre-exponential factor in cubic crystals can then be written as

$$D_0 = \frac{1}{6} \lambda^2 \times \nu_{eff}, \quad (5)$$

where λ is the jump length and ν_{eff} —the effective attempt frequency

$$\nu_{eff} = \nu_0 \times \exp\left(\frac{\Delta S_v^m(T)}{k_B}\right), \quad (6)$$

ν_0 —the actual attempt frequency of mono-vacancy diffusion jump.

The migration barrier for monovacancy diffusion is considered as the difference in Gibbs free energy G_v^m between the saddle-point and the equilibrium position, and can be expressed in terms of the migration enthalpy H_v^m and migration entropy S_v^m , which corresponds to the change in lattice vibrations, when diffusion jump occurs

$$\Delta G_v^m = \Delta H_v^m - T\Delta S_v^m. \quad (7)$$

Accordingly, the temperature variations of activation enthalpy and entropy are coupled via equation,

$$\frac{\delta\Delta H}{\delta T} = T \frac{\delta\Delta S}{\delta T}, \quad (8)$$

meaning that if ΔH is assumed temperature independent, consequently, so is ΔS —this assumption is valid for temperatures below $\approx 2/3$ of T_m , where only one vacancy diffusion mechanism plays important role. However, when $T > 2/3 T_m$ is reached, the effective ΔH_{eff} and ΔS_{eff} exhibit temperature dependence due to the contribution of the processes x with different diffusion activation parameters, $\Delta H_x(T)$ and $D_{0x}(S, T)$.

Formation and migration mechanisms of vacancies are not firmly established, especially at high temperatures, and have been studied in order to explain early self-diffusion experiments.⁴ Precise self-diffusion experimental measurements show that some FCC metals such as Ag, Cu, Au, Pt, and Ni^{5,6} and BCC metals Mo, Ta, V, and W^{4,7,8} exhibit non-Arrhenius behaviour of self-diffusion close to the melting point.

Several mechanisms have been proposed to interpret the slight upward curvature of the Arrhenius diagram, such as (1) simultaneous diffusion of monovacancies and larger vacancy clusters (divacancies), (2) self-interstitial atom (SIA) diffusion, (3) next-nearest neighbour jumps of vacancies, and (4) temperature dependence of vacancy formation and diffusion parameters.

First, as the binding energy for two W monovacancies, obtained by DFT and MD within this study, is close to 0 eV, we expect divacancy contribution in the increase of self-diffusion coefficient to play a minor role. Second, the formation energy of a SIA in W is over 9 eV (Refs. 9 and 10) making its thermodynamic contribution to self-diffusion negligible at any temperature. In the work by Satta *et al.*,¹¹ it was shown that the vacancy formation energy in W decreases somewhat at higher temperatures, which, according to their conclusions, explains partly, nevertheless not fully, the deviation from Arrhenius behaviour.

The available experimental data for diffusion in tungsten exists only for W self-diffusion.⁴ No experimental data on vacancy diffusion are found in literature but nevertheless monovacancy diffusion pre-exponential factors are used in numerous computational studies,^{12,13} being up to 3 orders of magnitude smaller than it should be according to our MD simulations with all 4 tested interatomic potentials.

In this paper, we simulate monovacancy diffusion to further elucidate the reasons for the super-exponential temperature dependence for self-diffusion in W. We also calculate the jump frequency for monovacancy diffusion to be used in multi-scale models, like kinetic monte carlo simulations and rate equations.^{14,15}

II. METHODS

Our modelling of monovacancy diffusion in W is based on density functional theory (DFT) and molecular dynamics (MD) techniques. We use MD code PARCAS¹⁶ (The main principles of the MD algorithms are presented in Refs. 17 and 18.) employing two types of semi-empirical potentials, embedded atom model (EAM),²¹ and Tersoff-Brenner-Type

bond-order potentials (BOPs)^{19,20,22} describing forces between interacting atoms. Potentials used in this study provide generally good description of W properties.

Three different MD simulation cell sizes, depending on the temperature, consisting of $4 \times 5 \times 6$, $8 \times 10 \times 12$, and $12 \times 14 \times 16$ unit cells in x, y, and z directions are used for MD simulations over a wide temperature range (from $0.35 T_m$ to T_m). It is tested that the size of the cell does not affect the monovacancy diffusion coefficient. Pressure during simulation is kept constant at 0 kBar. Temperatures lower than 1300 K are not investigated due to the limitations of MD simulation time scale.

The monovacancy position during simulation is tracked using Wigner-Seitz analysis and the diffusion coefficient is determined by the Einstein relation with improved accuracy,²³ as follows:

$$D = \frac{1}{N} \frac{\sum_i^N R_i^2(t)}{6 \sum_i^N t_i}, \quad (9)$$

$R_i^2(t)$ being the square displacement of the diffusing monovacancy, t —the diffusion time and N —the number of intervals the monovacancy path is divided into. In order to get sufficient monovacancy jump statistics, the total diffusion time is chosen from 20 ns at temperatures close to the melting point, up to 6000 ns at low temperatures (1300 K), where monovacancy jumps occur less frequent.

The DFT calculations were performed for determining the groundstate energies of the studied W mono-vacancy systems and the migration barriers between the different atomistic groundstate geometries. The Vienna Ab-Initio Simulation Package (VASP) was used in all of the DFT calculations.^{24–26} The electronic groundstate was calculated using projector-augmented wave (PAW) potentials^{27,28} as provided in VASP. The conjugate gradient algorithm was used for the groundstate volumetric and ionic relaxations. No symmetrizations were applied. The electron-exchange correlation was described with generalized gradient approximation using Perdew-Burke-Ernzerhof functionals.^{29,30} The partial occupancies were integrated with the Methfessel and Paxton method³¹ of the first order. A $3 \times 3 \times 3$ k-point mesh was sampled with Monkhorst and Pack scheme.³²

Supercell with 128 lattice sites was used for the $\langle 100 \rangle$ and $\langle 110 \rangle$ W monovacancy geometries. A larger supercell with 160 sites was used in the $\langle 111 \rangle$ geometry calculations. For all the geometries, once the groundstate energies were found, the monovacancy migration energetics was determined with the nudged elastic band (NEB) method.^{33,34} Fifteen intermediate images with two endpoint images were used in NEB for finding the geometries giving the minimum energy for the W monovacancy migration paths.

III. RESULTS AND DISCUSSION

Using MD methods, we simulate single vacancy diffusion over a wide temperature range, where monovacancy migrates due to thermal activation, allowing us to estimate

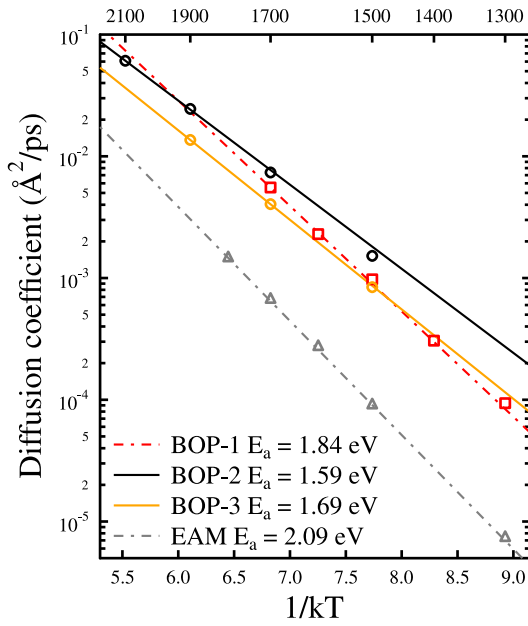


FIG. 1. Arrhenius diagram for W monovacancy diffusion at temperatures below $2/3 T_m$ (BOP-1, BOP-2, BOP-3, EAM).

diffusion related parameters. In this study, we determine the diffusion coefficients at different temperatures for four semi-empirical potentials: one EAM potential and three BOPs.

The Arrhenius fits to diffusion coefficients in Eq. (4) for temperatures below 2300 K obtained from MD simulations yields to the monovacancy migration energies from 1.59 to 2.09 eV, depending on the potential, the experimental value being 1.78 eV.² The results are presented as Arrhenius plots in Figure 1. The experimental and simulated melting points and diffusion parameters are summarized in Table I.

We proceed with using BOP-1 for further analysis, as it is the potential that gives the activation energy for monovacancy diffusion in best agreement with the experimental and DFT values.

Vacancies in the lattice move due to the exchange mechanism: tungsten atom, overcoming diffusion barrier, moves to an empty lattice site and the vacancy is considered to be moved one nearest neighbour (1NN) distance in the $\langle 111 \rangle$ direction. The jump frequency for monovacancy diffusion is calculated from Eq. (5) using the 1NN jump length: $\lambda = \sqrt{3}/2 \times a = 2.74 \text{ \AA}$ (a is the lattice constant in W $\sim 3.17 \text{ \AA}$) and the pre-exponential factor $\sim 1.5 \times 10^{-5} \text{ m}^2/\text{s}$ (from Table I).

The obtained jump frequency of about $1.2 \times 10^{15} \text{ Hz}$ is significantly larger than the value of 6×10^{12} used in the

TABLE I. Melting temperatures, diffusion activation energies, pre-exponential factors, and attempt frequencies for W.

Method	T_m (K)	E_a (eV)	D_0 (m^2/s)	ν (Hz)
Exp (Refs. 2 and 4)	3695	1.8	4.0×10^{-6a}	...
DFT (Refs. 3 and 18)	...	1.71, 1.78
BOP-1 (Ref. 17)	2750	1.84	1.5×10^{-5}	1.2×10^{15}
BOP-2 (Ref. 18)	4550	1.59	4.0×10^{-6}	3.2×10^{14}
BOP-3 (Ref. 20)	4550	1.69	4.2×10^{-6}	3.4×10^{14}
EAM (Ref. 19)	~ 3750 (Ref. 35)	2.09	1.0×10^{-5}	8.2×10^{14}

^aData extracted from self-diffusion experiments.

literature.¹³ This high jump frequency is quite unexpected considering that a vacancy jump in BCC metals occurs when any of the eight 1NN W atoms with an approximated jump frequency of $5 \times 10^{12} \text{ Hz}$ jump into the vacancy. Clearly, the mechanism how vacancy position changes needs to be investigated in more detail. When analyzing the vacancy positions closer, we discover that at higher temperatures an increasing number of the vacancy position changes are not 1NN jumps, but two or three atoms in the $\langle 111 \rangle$ row move towards the empty lattice position, i.e., the vacancy moves two or three nearest neighbour distances simultaneously.

Furthermore, in our simulations we see simultaneous movement of W atoms not only along the same $\langle 111 \rangle$ direction: a significant number of two nearest neighbour jumps of monovacancy occur first in $\langle 111 \rangle$ direction, then in either $\langle 1-1-1 \rangle$, $\langle -11-1 \rangle$, $\langle -1-11 \rangle$, giving the total displacement of $\approx 3.17 \text{ \AA}$ —later referred as $-L_A$, or in $\langle 11-1 \rangle$, $\langle 1-11 \rangle$, $\langle -111 \rangle$ direction, with total displacement $\approx 4.48 \text{ \AA}$ —referred as $-L_B$. The nearest and next-nearest neighbour jumps are illustrated in Figure 2.

The sum of all these jump contributions (1NN jumps, as well as the other diffusion mechanisms) explain the exceptionally high effective monovacancy jump frequency obtained from the MD simulations.

To attain the probability for jump mechanisms present, the migration barriers for 1-3NN jumps along the crowdion row, are calculated with DFT NEB method (shown in Figure 3), giving the energy barriers listed in Table II.

Moreover, to examine more closely the movement of the atoms during multiple nearest neighbour jumps of monovacancy, the detailed DFT NEB calculation for three nearest neighbour jump is shown in Figure 4. Visualized in dashed coloured lines are the pair distances of the three moving W atoms (denoted as W_1 , W_2 , W_3) together with the migration barrier.

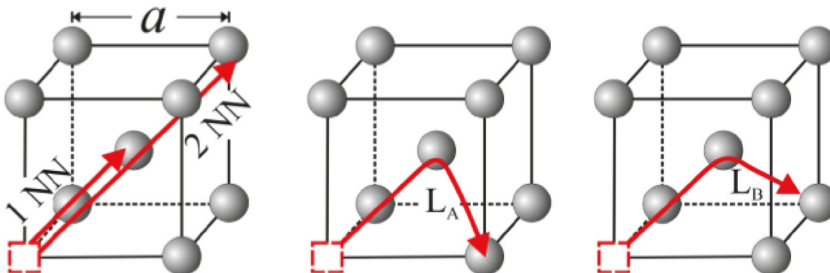


FIG. 2. Monovacancy jump paths in BCC metals.

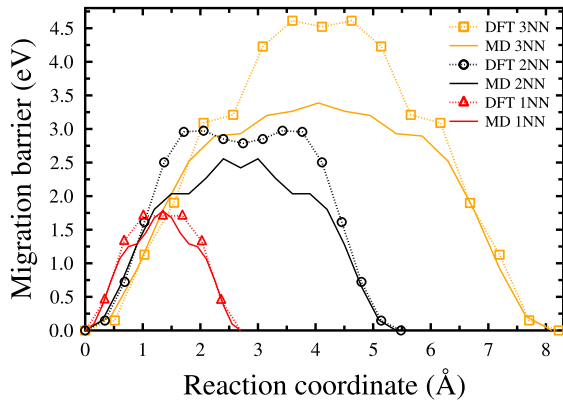


FIG. 3. DFT and MD (BOP-1) NEB calculation for monovacancy nearest (1NN), second (2NN) and third nearest neighbour (3NN) jumps in $\langle 111 \rangle$ direction. Note that the reaction coordinate value is right only at the end points.

Just before the 3NN jump, the both pair distances are the equilibrium 1NN distance of $\sim 2.7 \text{ \AA}$. Then the jump process is initiated by the increase of the distance W_1-W_2 , i.e., the W_1 atom moves towards the vacancy. This is followed by the both W_1 and W_2 atoms which move towards the vacancy, W_2 atom moving more until reaching NEB image 6 (Fig. 4), where the distance between W_1-W_2 is the 1NN distance and between W_2-W_3 the maximum of about $1.4 \times 1NN$ distance. The midway of the process, where the migration barrier is the highest, is then reached by movement of W_3 atom towards the vacancy. The migration process is then completed with the mirror movement of the three W atoms, resulting in that the monovacancy has made a 3NN jump. Similar cyclic atomic movement is seen for the 2NN jump.

The NEB calculations for the monovacancy L_A and L_B jumps give the lowest migration barrier of about 1.8 eV, being the same as for the 1NN jump. In this case, the movements would not be simultaneous, but two consecutive 1NN jumps. However, our MD simulations indicate that L_A and L_B monovacancy jumps occur simultaneously at high temperatures—this is confirmed by our NEB calculations, shown in Figure 5, where the possible MD NEB energy barriers are presented for the L_A jump. The dashed lines show the energy barriers where two W atoms move simultaneously, i.e., the monovacancy jump is one lattice constant in $\langle 100 \rangle$ direction. Similar results are also seen for the L_B jump in $\langle 110 \rangle$ direction.

The probabilities for different nearest neighbour jumps for single vacancy in W are calculated from MD simulations and shown in Table III, where we can see that already at $2/3$ of T_m , a significant number of vacancy jumps are larger than the 1NN jump, which gives evident contribution to the diffusion coefficient with different activation parameters,

TABLE II. DFT and MD NEB monovacancy migration barriers and distances in $\langle 111 \rangle$ direction.

Nr of jumps	1NN ($\sim 2.74 \text{ \AA}$)	2NN ($\sim 5.5 \text{ \AA}$)	3NN ($\sim 8.2 \text{ \AA}$)
DFT E_m	1.7 eV	2.9 eV	4.6 eV
MD E_m	1.8 eV	2.6 eV	3.4 eV

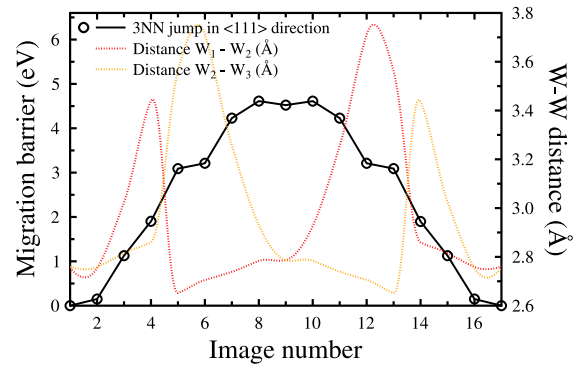


FIG. 4. DFT NEB calculation for monovacancy 3NN jump together with the pair distances between the three moving W atoms.

consequently curving the Arrhenius diagram at higher temperatures (shown in Figure 6). The total diffusion coefficient D_{tot} , taking into account all diffusion mechanisms, may be written

$$D_{tot} = D_1 \times \exp\left(\frac{-E_1}{k_B T}\right) + D_2 \times \exp\left(\frac{-E_2}{k_B T}\right) + D_3 \times \exp\left(\frac{-E_3}{k_B T}\right) + D_A \times \exp\left(\frac{-E_A}{k_B T}\right) + D_B \times \exp\left(\frac{-E_B}{k_B T}\right), \quad (10)$$

where D_x and E_x are pre-exponential factors and migration barriers, respectively, for $x=1$: 1NN jumps, $x=2$: 2NN, $x=3$: 3NN jumps, $x=A$: L_A jumps, and $x=B$: L_B jumps. Our DFT results also indicate that even a 3rd nearest neighbour jump is possible for the monovacancy at high temperatures, i.e., close to the T_m .

The migration enthalpy below $2/3$ of T_m of the W monovacancies is considered temperature independent, however, the contribution of additional vacancy diffusion mechanisms become more and more important at higher temperatures, thus, resulting in the temperature variation of effective migration enthalpy, shown in Figure 6—simulation points above 1900 K.

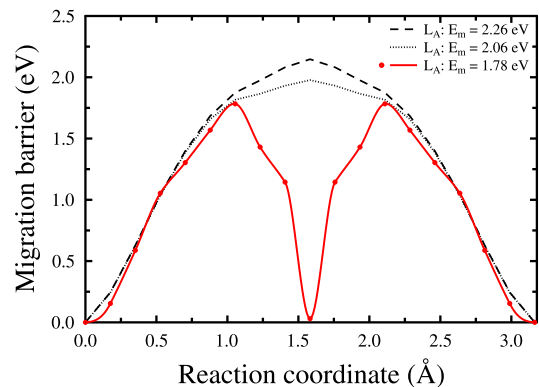


FIG. 5. MD NEB calculation for the L_A monovacancy jump. The possible higher migration barriers (dashed lines) show simultaneous movement of the two W atoms, while for the lowest energy barrier (solid line) there are two consecutive 1NN jumps. Note that the reaction coordinate value is right only at the end points.

TABLE III. Vacancy jump analysis at different temperatures with BOP-1 (Ref. 17): 1NN, 2NN 3NN nearest neighbour distance jumps in $\langle 111 \rangle$ direction, L_A jump of length $\sim 3.17 \text{ \AA}$, L_B jump of length $\sim 4.48 \text{ \AA}$.

Temp	1NN	2 NN	3 NN	L_A	L_B
1500 K	99.58%	0.42%	0%	0%	0%
1900 K	96.37%	2.35%	0.05%	0.16%	1.07%
2500 K	79.89%	6.77%	0.88%	2.83%	9.63%

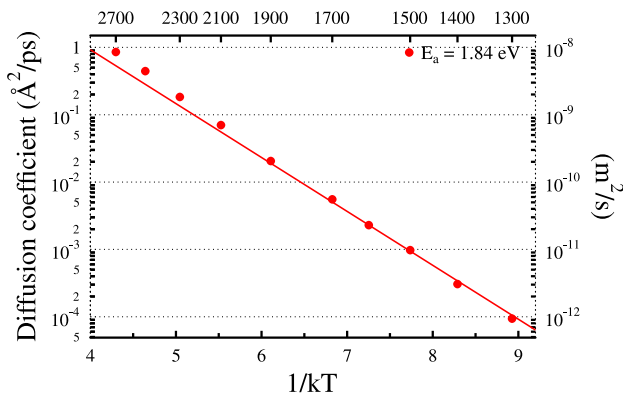


FIG. 6. Arrhenius diagram for W monovacancy diffusion (BOP-1). Fitted $D_0 = 1.5 \times 10^{-5} \text{ m}^2/\text{s}$, $E_a = 1.84 \text{ eV}$ —for temperatures 1300–1600 K, resulting in the attempt frequency $\nu = 1.2 \times 10^{15} \text{ Hz}$. The diffusion coefficient shows clear super-exponential behaviour at higher temperatures.

The experimental study of W vacancy migration and formation enthalpies³⁶ indicates the increase of apparent monovacancy migration enthalpy from $1.68 \pm 0.06 \text{ eV}$ at 1500 K to $2.02 \pm 0.05 \text{ eV}$ at 2600 K, which justifies our conclusion that this temperature dependence arises due to the onset of additional diffusion mechanisms with higher migration enthalpies, which can partly explain the upward curvature of W self-diffusion.⁴

Note that the number of 2NN, and especially 3NN jumps, given in Table III is larger than predicted by DFT as the corresponding MD migration barriers are underestimated as shown in Table II and Figure 3.

IV. CONCLUSIONS

We have used the MD and DFT methods to show that the monovacancy in W makes besides the expected nearest neighbour jumps in $\langle 111 \rangle$ direction, also longer jumps in $\langle 111 \rangle$, $\langle 100 \rangle$, and $\langle 110 \rangle$ directions. These additional jumps, together with temperature dependent vacancy formation energy,¹¹ could now explain the experimentally observed non-Arrhenius self-diffusion data in W,⁴ and probably also in other transition metals.³⁷ For the first time, the diffusion pre-exponential factor for W monovacancy diffusion is calculated and found to be more than two orders of magnitude higher than the values commonly used in computational studies. The use of this remarkably much higher jump frequency might have surprisingly large effects on the simulation results of different multi-scale models.

ACKNOWLEDGMENTS

This work, supported by the European Communities under the contract of Association between Euratom-Tekes, was carried out within the framework of the European Fusion Development Agreement (EFDA). Grants of computer time from the Center for Scientific Computing (CSC) in Espoo, Finland are gratefully acknowledged.

- ¹G. Neumann and C. Tuijn, *Self-Diffusion and Impurity Diffusion in Pure Metals: Handbook of Experimental Data* (Pergamon Press., 2008).
- ²K.-D. Rasch, R. W. Siegela, and H. Schultz, *Philos. Mag. A* **41**, 91 (1980).
- ³D. Nguyen-Manh, A. P. Horsfield, and S. L. Dudarev, *Phys. Rev. B* **73**, 020101 (2006).
- ⁴J. N. Mundy, S. J. Rothman, N. Q. Lam, H. A. Hoff, and L. J. Nowicki, *Phys. Rev. B* **18**, 6566 (1978).
- ⁵C. Herzig, H. Ecksele, W. Bussmann, and D. Cardis, *J. Nucl. Mater.* **69/70**, 61 (1978).
- ⁶R. P. Sahu, K. C. Jain, and R. W. Siegel, *J. Nucl. Mater.* **69/70**, 264 (1978).
- ⁷B. E. Pawel and T. S. Lundy, *J. Phys. Chem. Solids* **26**, 937 (1965).
- ⁸J. Pelleg, *Philos. Mag.* **29**, 383 (1974).
- ⁹K. Heinola and T. Ahlgren, *Phys. Rev. B* **81**, 073409 (2010).
- ¹⁰I. M. Neklyudov, E. V. Sadanov, G. D. Tolstolutskaia, V. A. Ksenofontov, T. I. Mazilova, and I. M. Mikhailovskij, *Phys. Rev. B* **78**, 115418 (2008).
- ¹¹A. Satta, F. Willaime, and S. de Gironcoli, *Phys. Rev. B* **57**(18), 11184 (1998).
- ¹²M. J. Caturla, N. Soneda, E. Alonso, B. D. Wirth, T. Diaz de la Rubia, and J. M. Perlado, *J. Nucl. Mater.* **276**, 13 (2000).
- ¹³C. S. Becquart, C. Domain, U. Sarkar, A. DeBacker, and M. Hou, *J. Nucl. Mater.* **403**, 75 (2010).
- ¹⁴A. D. Brailsford and R. Bullough, *Philos. Trans. R. Soc. London* **302**, 87–137 (1981).
- ¹⁵A. B. Bortz, M. H. Kalos, and J. L. Lebowitz, *J. Comput. Phys.* **17**, 10–18 (1975).
- ¹⁶K. Nordlund, 2006 PARCAS Computer code; private communication.
- ¹⁷K. Nordlund, M. Ghaly, R. S. Averback, M. Caturla, T. Diaz de la Rubia, and J. Tarus, *Phys. Rev. B* **57**, 7556 (1988).
- ¹⁸M. Ghaly, K. Nordlund, and R. S. Averback, *Philos. Mag. A* **79**, 795 (1999).
- ¹⁹N. Juslin, P. Erhart, P. Träskelin, J. Nord, K. O. E. Henriksson, K. Nordlund, E. Salonen, and K. Albe, *J. Appl. Phys.* **98**, 123520 (2005).
- ²⁰T. Ahlgren, K. Heinola, N. Juslin, and A. Kuronen, *J. Appl. Phys.* **107**, 033516 (2010).
- ²¹P. M. Derlet, D. Nguyen-Manh, and S. L. Dudarev, *Phys. Rev. B* **76**, 054107 (2007).
- ²²X.-C. Li, Xiaolin Shu, Y.-N. Liu, F. Gao, and G.-H. Lu, *J. Nucl. Mater.* **408**, 12 (2011).
- ²³M. W. Guinan, R. N. Stuart, and J. R. Borg, *Phys. Rev. B* **15**, 699 (1977).
- ²⁴G. Kresse and J. Hafner, *Phys. Rev. B* **47**, 558 (1993).
- ²⁵G. Kresse and J. Hafner, *Phys. Rev. B* **49**, 14251 (1994).
- ²⁶G. Kresse and J. Furthmüller, *Phys. Rev. B* **54**, 11169 (1996).
- ²⁷P. E. Blöchl, *Phys. Rev. B* **50**, 17953 (1994).
- ²⁸G. Kresse and D. Joubert, *Phys. Rev. B* **59**, 1758 (1999).
- ²⁹J. P. Perdew, K. Burke, and M. Ernzerhof, *Phys. Rev. Lett.* **77**, 3865 (1996).
- ³⁰Y. Zang and W. Yang, *Phys. Rev. Lett.* **80**, 890 (1998).
- ³¹M. Methfessel and A. T. Paxton, *Phys. Rev. B* **40**, 3616 (1989).
- ³²H. Monkhorst, *Phys. Rev. B* **13**, 5188 (1976).
- ³³G. Mills, H. Jónsson, and G. K. Schenter, *Surf. Sci.* **324**, 305 (1995).
- ³⁴H. Jónsson, G. Mills, and K. W. Jacobsen, *Classical and Quantum Dynamics in Condensed Phase Simulations*, edited by B. J. Berne, G. Ciccotti, and D. F. Coker (World Scientific, Singapore, 1998), pp. 385–404.
- ³⁵J. Fikar and R. Schäublin, *J. Nucl. Mater.* **97**, 386 (2009).
- ³⁶J. N. Mundy, S. T. Ockers, and L. C. Smedskjaer, *Philos. Mag. A* **56**, 851 (1987).
- ³⁷K. Maier, H. Mehrer, and G. Rein, *Z. Metallkd.* **170**, 271 (1979).